Computational Mechanics (1993) 12, 255–268

Computational Mechanics

An adaptive mesh refinement technique for two-dimensional shear band problems

R. C. Batra and **J. Hwang**

Department of Mechanical and Aerospace Engineering and Engineering Mechanics, University of Missouri-Rolla, Rolla, MO 65401-0249, USA

Abstract. We have developed an adaptive mesh refinement technique that rezones the given domain for a fixed number of quadrilateral elements such that fine elements are generated within the severely deformed region and coarse elements elsewhere. Loosely speaking, the area of an element is inversely proportional to the value of the deformation measure at its centroid. Here we use the temperature rise at a material point to gauge its deformations which is reasonable for the shear band problem since the material within the shear band is deformed intensely and is heated up significantly. It is shown that the proposed mesh refinement technique is independent of the initial starting mesh, and that the use of an adaptively refined mesh gives thinner shear bands, and sharper temperature rise and the growth of the second invariant of the plastic strain-rate within the band as compared to that for a fixed mesh having the same number of nodes. The method works well even when the deformation localizes into more than one narrow region.

1 Introduction

Most of the previous two-dimensional numerical studies of shear bands have used a fixed finite element mesh (e.g., see Batra and Liu 1989; Needleman 1989; Batra and Zhu 1991), an exception seems to be the recent work of Batra and Ko (1992) who developed a mesh refinement technique that generates fine triangular elements in the severely deforming region and coarse elements elsewhere. They added more elements to the region as the localization of the deformation into a narrow band progressed. Assuming that enough core storage is available in the computer being used, this technique enables one to resolve sharp gradients of the deformation within the severely deforming region in as great a detail as desired. Of course, adding new elements increases the computational cost, necessitates the generation of a new element topology, and may eventually make the system of algebraic equations to be solved ill-conditioned and/or extremely stiff. One could circumvent this by limiting the ratio of the largest to the smallest element in the mesh. Another way to refine a mesh is to use a fixed number of elements and nodes, and adjust the locations of nodes so as to concentrate fine elements in the severely deforming regions and coarse elements elsewhere. It keeps the element topology fixed and thus requires less bookkeeping and can be easily implemented in an existing code. It is shown that the mesh so generated is independent of the starting mesh and can adequately delineate the localization of the deformation into narrow bands.

For one-dimensional problems, Drew and Flaherty (1984) have used the moving grid method to develop an adaptive finite element code that locates regions with large gradients and concentrates fine elements there in order to minimize approximately the discretization error per time step. Pervaiz and Baron (1988) have discussed an adaptive technique which refines the spatial and/or temporal grid whenever preselected gradients exceed the threshold levels and have applied it to study quasi-one-dimensional unsteady flow problems involving finite rate chemistry. Batra and Kim (1990) developed an adaptive mesh refinement technique that distributes uniformly the scaled residuals of equations expressing the balance of linear momentum and the balance of internal energy. They subdivided elements having large scaled residuals and noted that large values of the scaled residuals occurred, in general, in non-overlapping regions. Their technique did not combine elements with large scaled residuals, and thus did not result in an optimum mesh.

We refer the reader to Safjan et al. (1991) and Zienkiewicz and Zhu (1991) for an extensive list of references on adaptive mesh refinement, to Batra and Zhu (1991) for several references on adiabatic shear banding, and to the recent book by Bai and Dodd (1992) for a summary of the work completed on adiabatic shear banding till 1989.

2 Formulation of the shear band problem

We study plane strain thermomechanical deformations of a thermally softening viscoplastic prismatic body of square cross-section, and use a fixed set of rectangular Cartesian coordinates with origin at its centroid (see Fig. 1). In terms of the referential description, governing equations are:

$$(J)^{\cdot} = 0, \quad \rho \dot{v}_i = T_{i\alpha,\alpha}, \quad \rho \dot{e} = -Q_{\alpha,\alpha} + T_{i\alpha} v_{i,\alpha}, \tag{1–3}$$

where

$$J = \det F_{i\alpha}, \quad F_{i\alpha} = x_{i,\alpha} \equiv \partial x_i / \partial X_\alpha, \tag{4}$$

x_i is the present position of a material particle that occupied place X_α in the reference configuration, ρ its mass density, v_i its present velocity, a superimposed dot signifies the material time derivative, a comma followed by an index $\alpha(i)$ stands for partial derivative with respect to X_α (x_i), a repeated index implies summation over the range of the index, $\mathbf{T}$ is the first Piola–Kirchhoff stress tensor, e is the specific internal energy, and $\mathbf{Q}$ is the heat flux per unit undeformed area. Equation (1) implies that the deformations are isochoric. The balance laws (1)–(3) are supplemented by the following constitutive relations

$$\sigma_{ij} = -p\delta_{ij} + 2\mu D_{ij}, \quad T_{i\alpha} = X_{\alpha,j}\sigma_{ij}, \quad 2\mu = \frac{\sigma_o}{\sqrt{3}I}(1 + bI)^m \left(1 + \frac{\psi}{\psi_o}\right)^n (1 - v\theta), \quad \dot{e} = c\dot{\theta}, \tag{5, 6}$$

$$Q_\alpha = X_{\alpha,j} q_j, \quad q_i = -k\theta_{,i}, \quad \dot{\psi} = \sigma_{ij} D_{ij} \bigg/ \left(1 + \frac{\psi}{\psi_o}\right)^n, \quad 2D_{ij} = v_{i,j} + v_{j,i}, \quad 2I^2 = D_{ij}D_{ij}. \tag{7, 8}$$

Here $\boldsymbol{\sigma}$ is the Cauchy stress tensor, p the hydrostatic pressure not determined by the deformation history of the material point, $\mathbf{D}$ the strain-rate tensor, σ_o the yield stress of the material in a quasistatic simple tension or compression test conducted at the room temperature, parameters b and m characterize the strain-rate sensitivity of the material, ψ_o and n its strain-hardening, v is the thermal softening coefficient, c the specific heat, k the thermal conductivity, and θ equals the temperature rise of a material particle. All of the material parameters are assumed to be independent of the temperature. Here we have neglected elastic deformations of the body since our

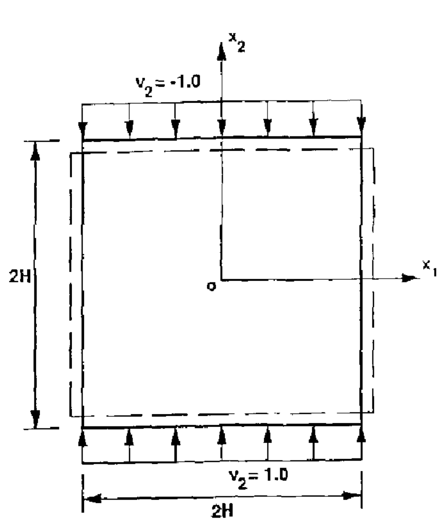

Fig. 1. A schematic sketch of the problem studied

interest is to study intense plastic deformations within the shear band. Also, all of the plastic working has been assumed to be converted into heating of the body.

We nondimensionalize variables by scaling stress like quantities by σ_o, time by H/v_o, length by H, and temperature by the reference temperature θ_r defined as

$$\theta_r = \sigma_o/(\rho c). \tag{9}$$

Here 2H is the height of the square block and v_0 the steady value of the velocity applied to the top and bottom surfaces in the x_2-direction. Henceforth we use nondimensional variables only and indicate them by the same symbols as those used for dimensional variables.

We assume that the initial and boundary conditions are such that the deformations of the block are symmetrical about the horizontal and vertical centroidal axes, and study deformations of the material in the first quadrant. We take all four surfaces of the region studied to be thermally insulated and free of tangential tractions. Because of the assumed symmetry of deformations, the normal velocity is zero on the left and bottom surfaces. The right vertical surface is taken to be free of normal tractions also, and a uniform vertically downward velocity of unit magnitude is applied on the top surface. For the initial conditions, we take

$$v_1(\mathbf{x},0) = x_1, \quad v_2(\mathbf{x},0) = -x_2, \tag{10.1}$$

$$\begin{aligned}\theta(\mathbf{x},0) &= \theta_o + \varepsilon(1-r^2)^9 e^{-5r^2}, \quad r^2 \equiv X_1^2 + X_2^2 \leqq 1,\\ &= \theta_o, \quad r > 1.\end{aligned} \tag{10.2}$$

That is, the transients have died out. It is highly unlikely that the transients will die out simultaneously throughout the body. However, the assumption is justified on the grounds that it does not affect the qualitative nature of results and reduces significantly the CPU effort necessary to solve the problem. The initial temperature distribution (10.2) models a material inhomogeneity; the height ε of the temperature bump can be thought of as representing the strength of the singularity.

The problem formulated above is highly nonlinear. We assume that it has a solution and find its approximation by the finite element method. We use four-noded quadrilateral elements, take the hydrostatic pressure to be constant within each element, and use 2×2 Gauss quadrature rule to evaluate various integrals over an element, and the lumped mass matrix obtained by employing the special lumping technique (e.g. see Hughes (1987)). The Galerkin approximation of the governing equations gives a set of coupled highly nonlinear ordinary differential equations (ODEs) for nodal values of two components of the velocity, temperature, internal variable ψ, and the values of the hydrostatic pressure p within each element. The ODEs are integrated by using the trapezoidal rule, hydrostatic pressure p is eliminated at the element level, and the nonlinear algebraic equations are solved iteratively by using one of the following two convergence criteria at each node point:

$$\frac{|\Delta v_1|}{|v_1|} + \frac{|\Delta v_2|}{|v_2|} + \frac{|\Delta\theta|}{\theta} + \frac{|\Delta\psi|}{\psi} \leqq \varepsilon_1, \qquad |\Delta v_1| + |\Delta v_2| + |\Delta\theta| + |\Delta\psi| \leqq \varepsilon_2. \tag{11.1, 11.2}$$

Here ε_1 and ε_2 are preassigned small numbers, and $\Delta\theta$ equals the difference in the nodal values of θ during two successive iterations within the same time increment. At boundary points where v_1 or v_2 is prescribed to be zero, Eq. (11.1) is not valid.

3 Adaptive mesh refinement technique

Here we discuss a mesh refinement technique in which the total number of elements, nodes and the element connectivity are kept fixed. The nodes are repositioned so that

$$a_e = \int_{\Omega_e} \eta \, d\Omega, \quad e = 1, 2, \ldots, n_{el}, \tag{12}$$

is nearly the same for each element Ω_e. In (12), η is a measure of the deformation such as the second invariant of the strain-rate tensor, temperature rise θ, the equivalent plastic strain, or the internal variable ψ, n_{el} equals the number of elements desired in the mesh and Ω_e is one of the elements. Our reason for making a_e the same over each element Ω_e is that within the region of localization of the deformation values of η are expected to be very high as compared to those in the remaining region. The refined mesh will depend upon what deformation measure is associated with η; here we take η to be the temperature rise θ.

Having solved the problem on an initial mesh we refine it as follows. We begin with either the horizontal boundary or the vertical one and relocate nodes on it according to the criterion described below. To be definite, let us begin with the left vertical edge. After having repositioned nodes on it we do the same on the almost vertical curve that passes through nodes next to the left vertical side, and continue the process till we reach the right vertical edge. The procedure is then repeated beginning with the top or bottom horizontal edge and going to the other end.

Referring to Fig. 2, let AB be the curve on which nodes are to be relocated. We plot the temperature distribution on AB with abscissa as the distance of a point from A measured along AB and ordinate as the temperature at that point. Values of temperature at numerous points on AB are obtained by linear interpolation from the values at node points. If S equals the total area under the curve, the approximate location s_n^a of the nth node on AB is given by

$$\int_{s_{n-1}}^{s_n^a} \theta \, ds = \frac{S}{N_{es}}, \tag{13}$$

where N_{es} equals the number of elements on AB. We reposition the node to the interpolation point immediately to the left of its approximate location determined from Eq. (13). In Fig. 2c, the position of a node as found from Eq. (13) is shown by a superimposed prime, and its relocation in Fig. 2d by superimposed two primes. Since the end points on AB are kept fixed, the aforestated procedure can be employed by starting from either A or B. Note that when nodes on an approximate horizontal curve are relocated, positions of nodes A and B will change.

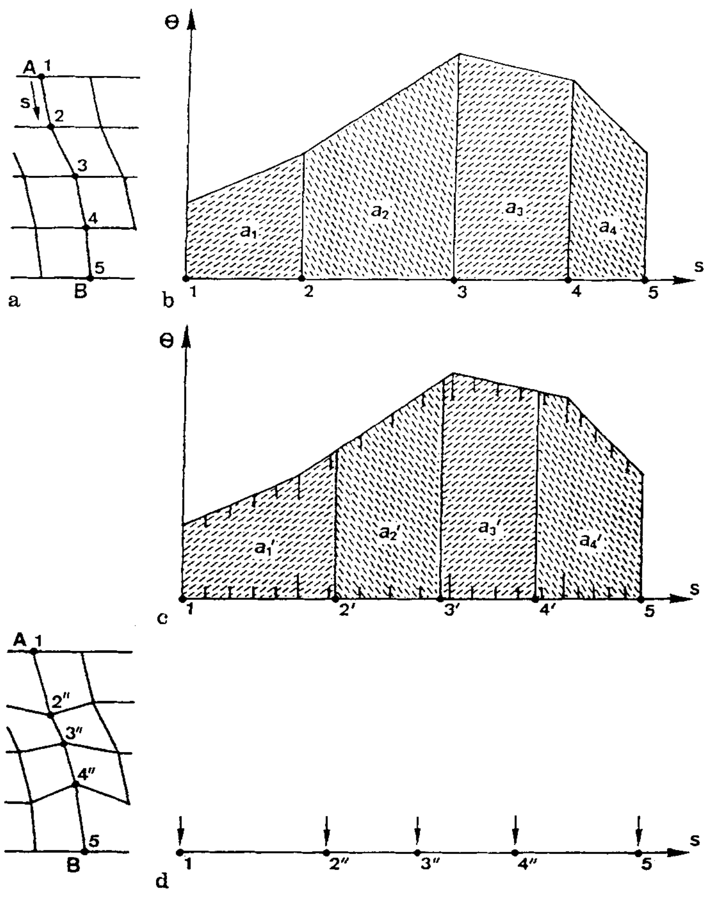

Fig. 2. **a** Curve AB on which nodes are to be relocated. **b** Temperature distribution on curve AB on which nodes are to be repositioned. **c** Temporary position on curve AB of relocated nodes. **d** Repositioned nodes on curve AB

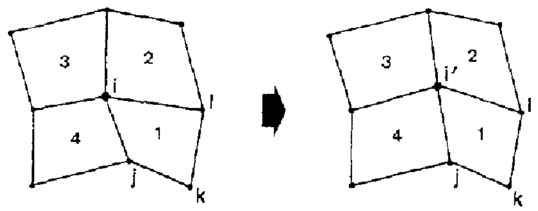

Fig. 3. Relocation of an interior node to smoothen out the generated mesh

The quadrilateral elements produced by the aforestated simple technique are not always well shaped in the sense that one of the interior angles may be either too small or too large. It usually happens in regions where the element size varies noticeably. We use the mesh smoothing method of Zhu et al. (1991) to improve upon the shapes of quadrilateral elements. Each internal node is repositioned to the centroid of the polygon formed by all of the elements meeting at the node. As illustrated in Fig. 3, the internal node i is moved to i' with coordinates given by

$$x_i' = \frac{1}{4M} \sum_{a=1}^{M} (x_j + 2x_k + x_l)_a, \quad y_i' = \frac{1}{4M} \sum_{a=1}^{M} (y_j + 2y_k + y_l)_a, \tag{14}$$

where M is the number of elements sharing node i. After having relocated all of the internal nodes, the element shapes are checked to see if all interior angles of every element are between 20° and 160°. If not, the nodes are repositioned according to Eq. (14) till such is the case. For the problems studied herein, the mesh smoothing procedure had to be applied atmost three times to generate a satisfactory mesh. Because of the smoothening of the mesh, the value of a_e defined by Eq. (12) is only approximately the same for all elements in the mesh.

4 Results and discussion

In order to illustrate the aforestated mesh refinement technique we compute results for the shear band problem with various variables assigned the following values.

$$b = 10000\,\text{sec}, \quad v = 0.0222\,^\circ\text{C}^{-1}, \quad \sigma_0 = 333\,\text{MPa}, k = 49.22\,\text{Wm}^{-1}\,^\circ\text{C}^{-1},$$
$$c = 473\,\text{Jkg}^{-1}\,^\circ\text{C}^{-1}, \quad \rho = 7860\,\text{kg}\,\text{m}^{-3}, \quad m = 0.025, \quad n = 0.09,$$
$$\psi_0 = 0.017, \quad H = 5\,\text{mm}, \quad v_0 = 25\,m/s, \quad \varepsilon = 0.2, \quad \varepsilon_1 = 10^{-3}, \quad \varepsilon_2 = 10^{-3}, \quad \theta_0 = 0. \tag{15}$$

These values except that for v are for a typical steel and were also used by Batra and Ko (1992). Note that here we also account for the work hardening of the material through the internal variable ψ. Values of parameters given in (15) imply that the average strain-rate equals $5000\,\text{sec}^{-1}$, $\theta_r = 89.6\,^\circ$C, and the nondimensional melting temperature equals 0.503. The higher values of v and ε speed up the initiation of a shear band and cut down significantly the CPU time required to study the problem without affecting the qualitative nature of results. The test data to find values of material parameters at strain-rates, strains and temperatures likely to occur in a shear band is not currently available, and a quantitative comparison of computed results with test findings is still not feasible.

Figure 4a shows the initial mesh consisting of 400 uniform elements, the generated refined meshes when the temperature θ at the centroid equalled 0.25, 0.35, and 0.45 are plotted in Figs. 4b, 4c, and 4d, respectively; the mesh was also refined when θ at the centroid reached 0.30 and 0.40, but these are not depicted in the figure for the sake of brevity. We choose to refine the mesh for equal increments of the temperature rise. However, other criteria such as the second invariant I of the strain-rate tensor attaining certain values, or equal increments in the value of ψ would be equally good. The meshes shown in Fig. 4 vividly reveal that the aforestated refinement technique generated a nonuniform mesh with finer elements in the severely deformed region and coarse elements elsewhere. The mesh smoothing criterion (14) had to be applied atmost three times to satisfy the requirement that the interior angles of every quadrilateral element be between 20° and 160°. We note that the mesh generation scheme does not impose any restriction on the ratio of

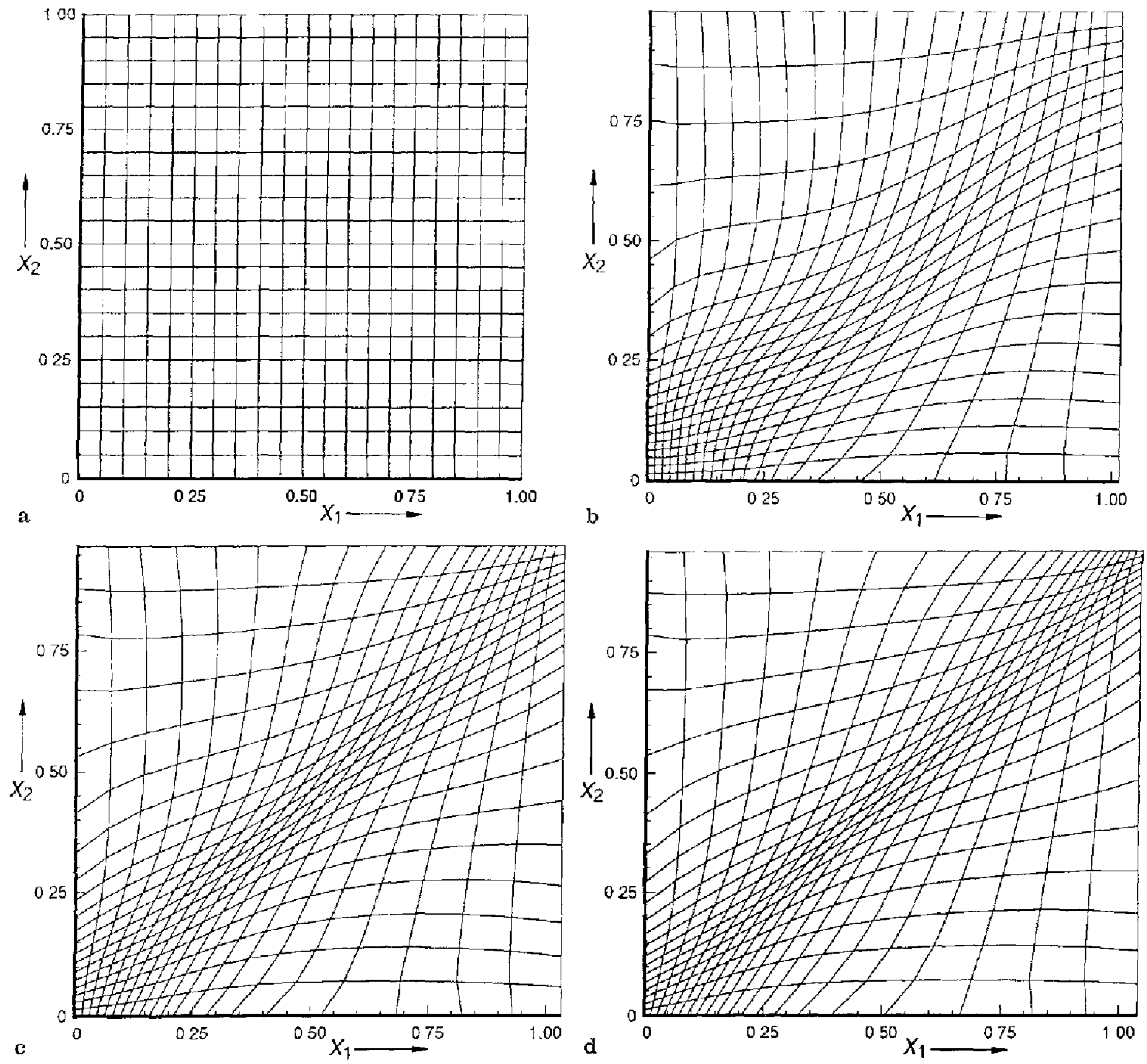

Fig. 4. **a** Initial uniform mesh of 400 elements. **b–d** Finite element meshes generated by using the mesh refinement technique when the temperature at the center of the specimen reached 0.25, 0.35, and 0.45

the area of the largest to that of the smallest element in the mesh. Even though this did not cause an unduly skewed mesh to be generated for the present problem, in other situations such a restriction may be necessary. One could avoid this either by having more elements in the initial mesh or by adding more elements at a few intermediate stages. The latter would necessitate the creation of a new element topology.

Figure 5 exhibits, in the deformed configuration, contours of the second invariant I of the deviatoric strain-rate tensor when the average strain $\gamma_{avg} = 0.0166$, 0.0352, and 0.044. These evidence that as the block continues to be deformed, the deformation localizes into an increasingly narrower band. The contours of I in the deformed configuration at $\gamma_{avg} = 0.044$ obtained by using a fixed mesh of initially 400 uniform elements plotted in Fig. 5d affirm the advantage of using an adaptively refined mesh. Not only the computed peak values of I within the band are higher for the refined mesh, the width of the region of localization is much narrower as compared to that obtained with a fixed mesh. From these contours one can estimate the band centerline to be the curve CED shown in Fig. 6a. In Figs. 6b and 6c, we have exhibited the variation, at different times, of the temperature rise θ and the second invariant I of the deviatoric strain-rate tensor on line AB that is perpendicular to the estimated band centerline and is shown in Fig. 6a. These plots confirm

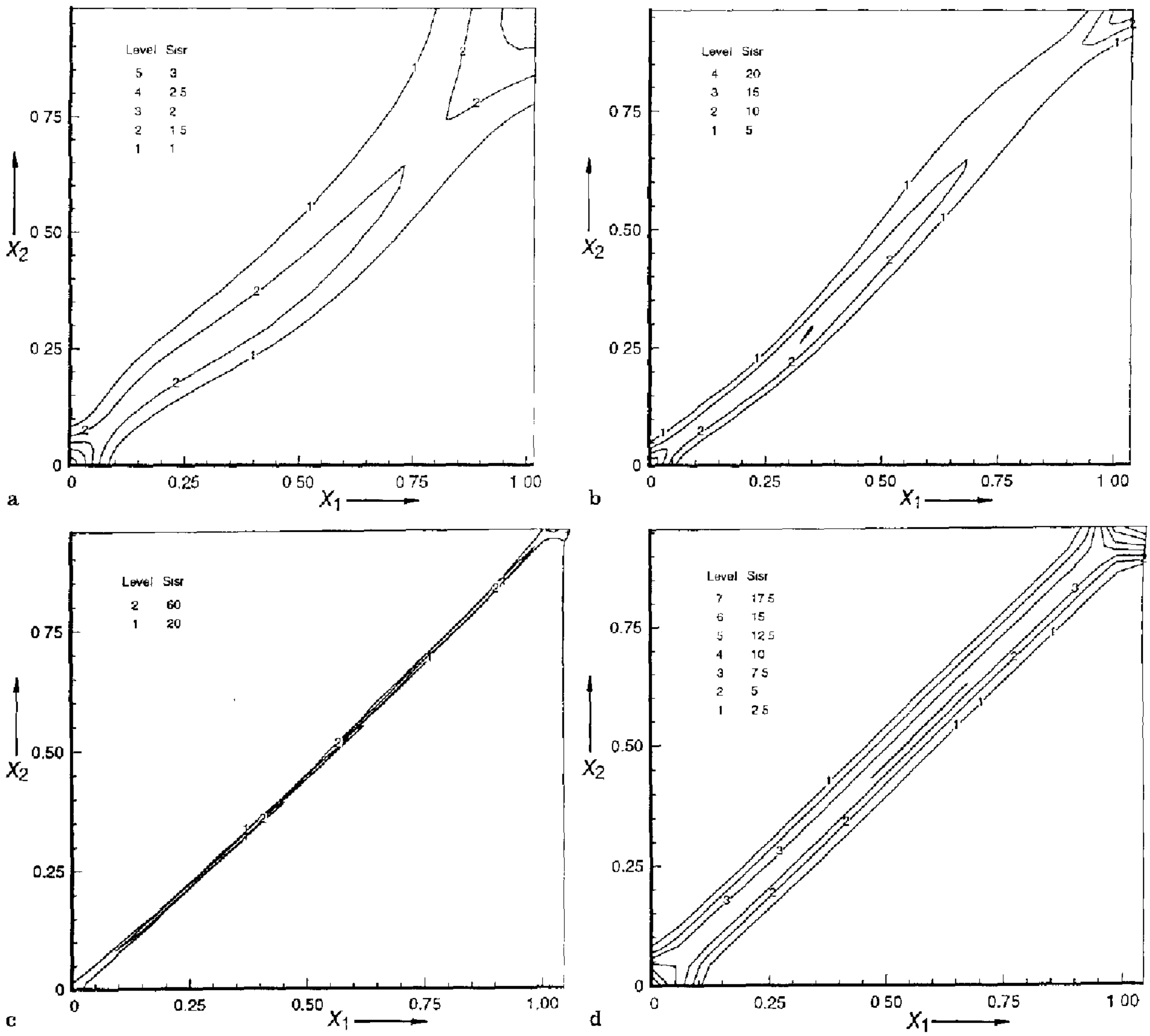

Fig. 5. a–c Contours of the second invariant I of the deviatoric strain-rate tensor at $\gamma_{avg} = 0.0166, 0.0352$, and 0.044. **d** Contours of the second invariant I of the deviatoric strain-rate tensor at $\gamma_{avg} = 0.044$ for a fixed mesh of 400 elements

the localization of the deformation into a narrow band as the block continues to be compressed. We note that the temperature rise θ is a measure of the total plastic work done at a point since the final nondimensional time of 0.044 equals 8.8 μs and the heat conducted away from a point during that interval is indeed minuscule. Thus, not only the accumulated deformation within the band is large, the material there is deforming severely at $t = 0.044$ as indicated by the high values of I there.

In Fig. 7 we have plotted for the fixed uniform mesh and for the adaptively refined mesh the evolution at the origin of the temperature rise, the second invariant I of the deviatoric strain-rate tensor and the effective stress s_e defined as

$$s_e = \sqrt{\frac{2}{3}}(1 - v\theta)(1 + bI)^m(1 + \psi/\psi_0)^n. \tag{16}$$

It is clear that the rates of growth of θ and I and the rate of drop of s_e at the origin are sharper for the refined mesh as compared to that for the fixed mesh with the same number of nodes. Computations were stopped when the temperature at the origin reached the presumed melting temperature of the material. There is no assurance that the computed results are optimum for the

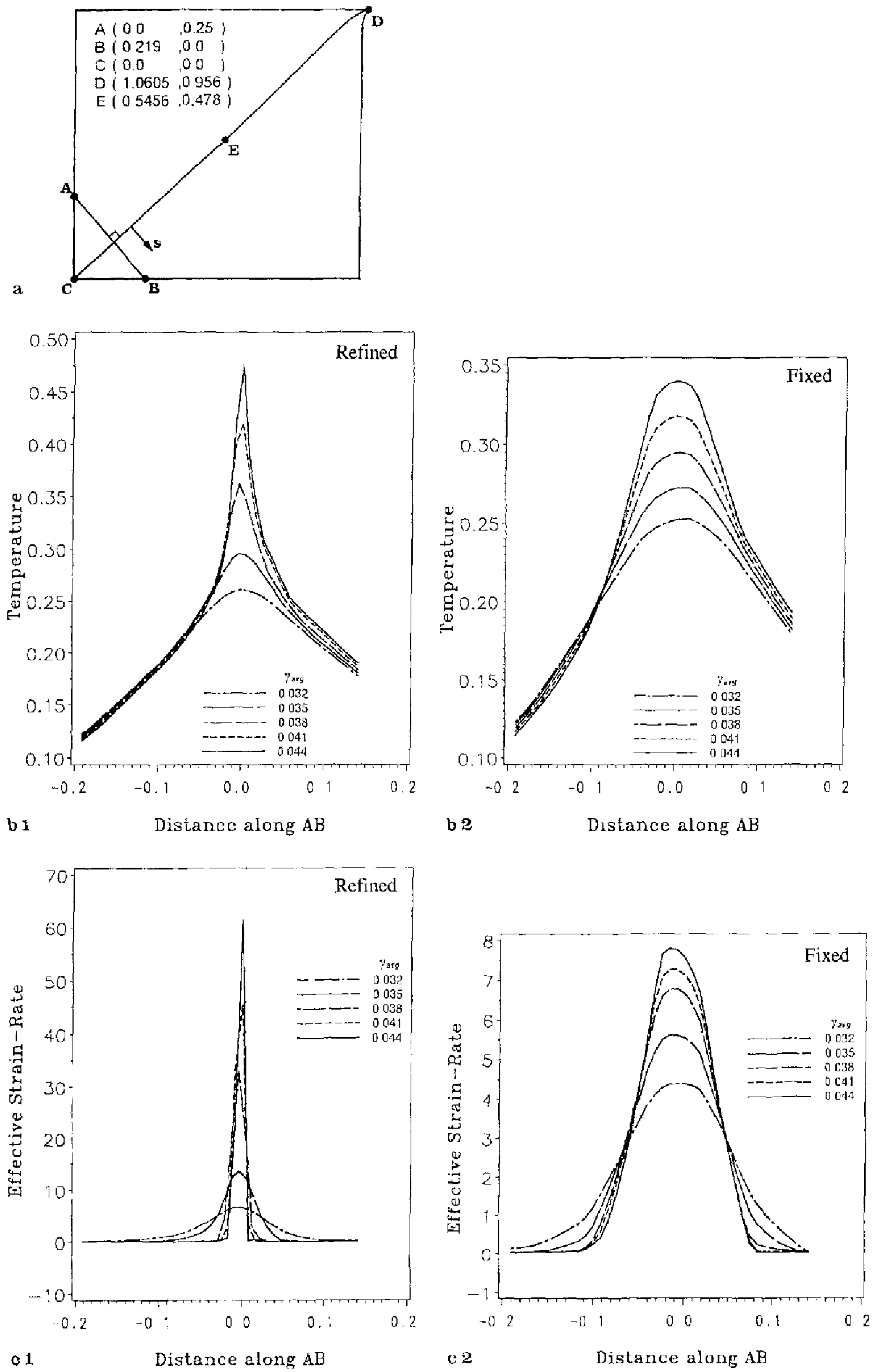

Fig. 6. **a** Estimated centerline of the shear band, and location of the transverse line AB. **b–c** variation at $\gamma_{avg} = 0.032, 0.035, 0.038, 0.041$, and 0.044 of the temperature rise θ and the second invariant I of the deviatoric strain-rate tensor on line AB

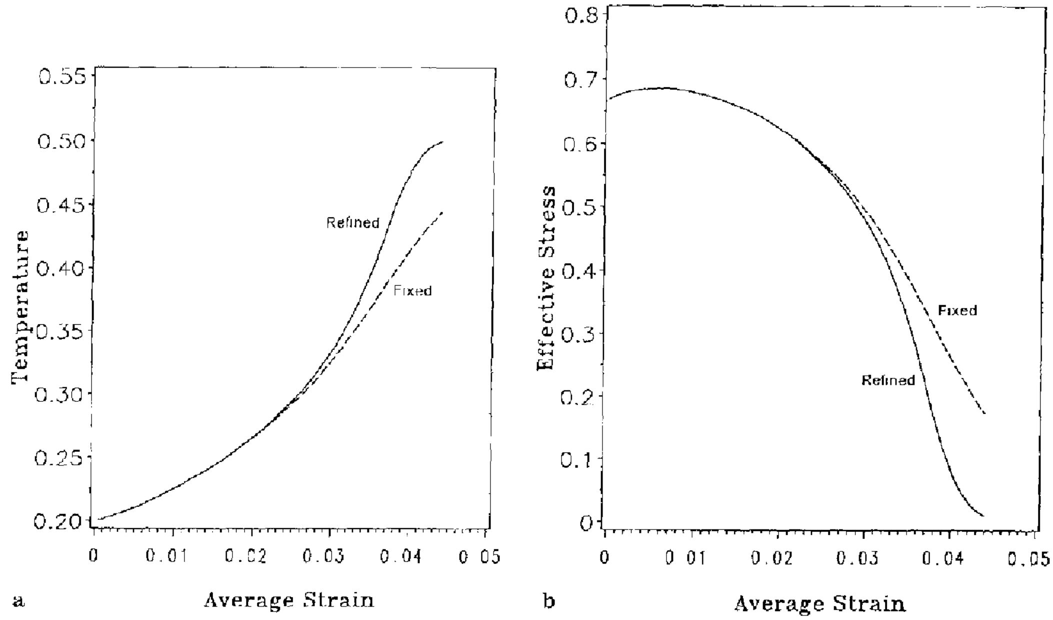

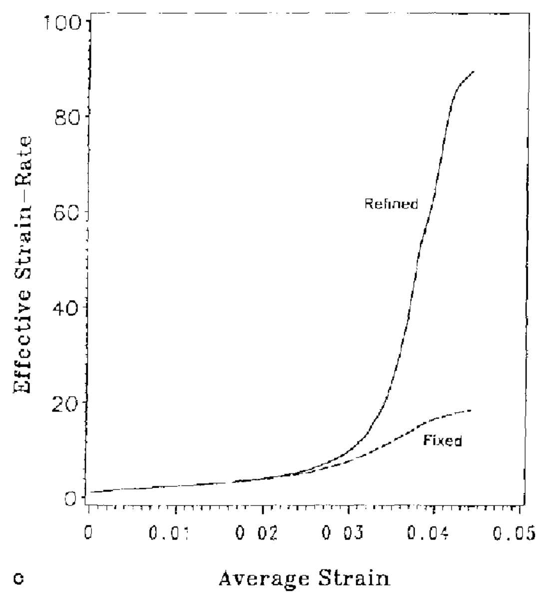

Fig. 7a–c. Evolution at the origin of the temperature rise, the second invariant I of the deviatoric strain-rate tensor, and the effective stress for a fixed mesh and for an adaptively refined mesh. I is labelled as the effective strain-rate in the figure

given number of nodes since they may also depend upon the finite element basis functions used to approximate the solution of the problem. For the refined mesh the second invariant of the deviatoric strain-rate tensor at the origin seems to reach a plateau due to the temperature there approaching the melting point of the material. Once that happens, the effective stress there vanishes. However, the surrounding material still contributes to the strength of the body.

We now investigate the improvement, if any, in the quality of the approximate solution obtained by refining the mesh adaptively. Since the analytical solution of the problem is unknown and there is no hope of finding one in the near future, we compare the approximate solution with a higher-order approximate solution (Hinton and Campbell 1974) obtained by smoothening out the computed solution. Let g be one of the variables to be smoothened. For the four-noded quadrilateral element, we write

$$g(\xi,\eta) = a + b\xi + c\eta + d\xi\eta \tag{17}$$

where (ξ,η) are the coordinates of a point with respect to a set of local coordinate axes, and constants a, b, c, and d are determined from the values of g at the four quadrature points within

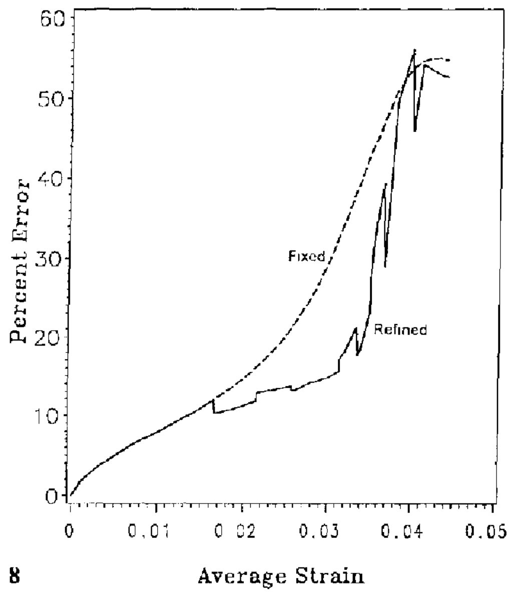

8

Figs. 8 and 9. 8 Comparison of the error in the approximate solution computed with a fixed mesh and an adaptively refined mesh. In each case, the error is determined by comparing the computed solution with a higher-order approximate solution. **9a–d a** Initial nonuniform mesh of 400 elements. **b** Comparison of the evolution at the origin of the temperature rise, second invariant of the deviatoric strain-rate tensor and the effective stress obtained by using meshes refined from two different initial meshes

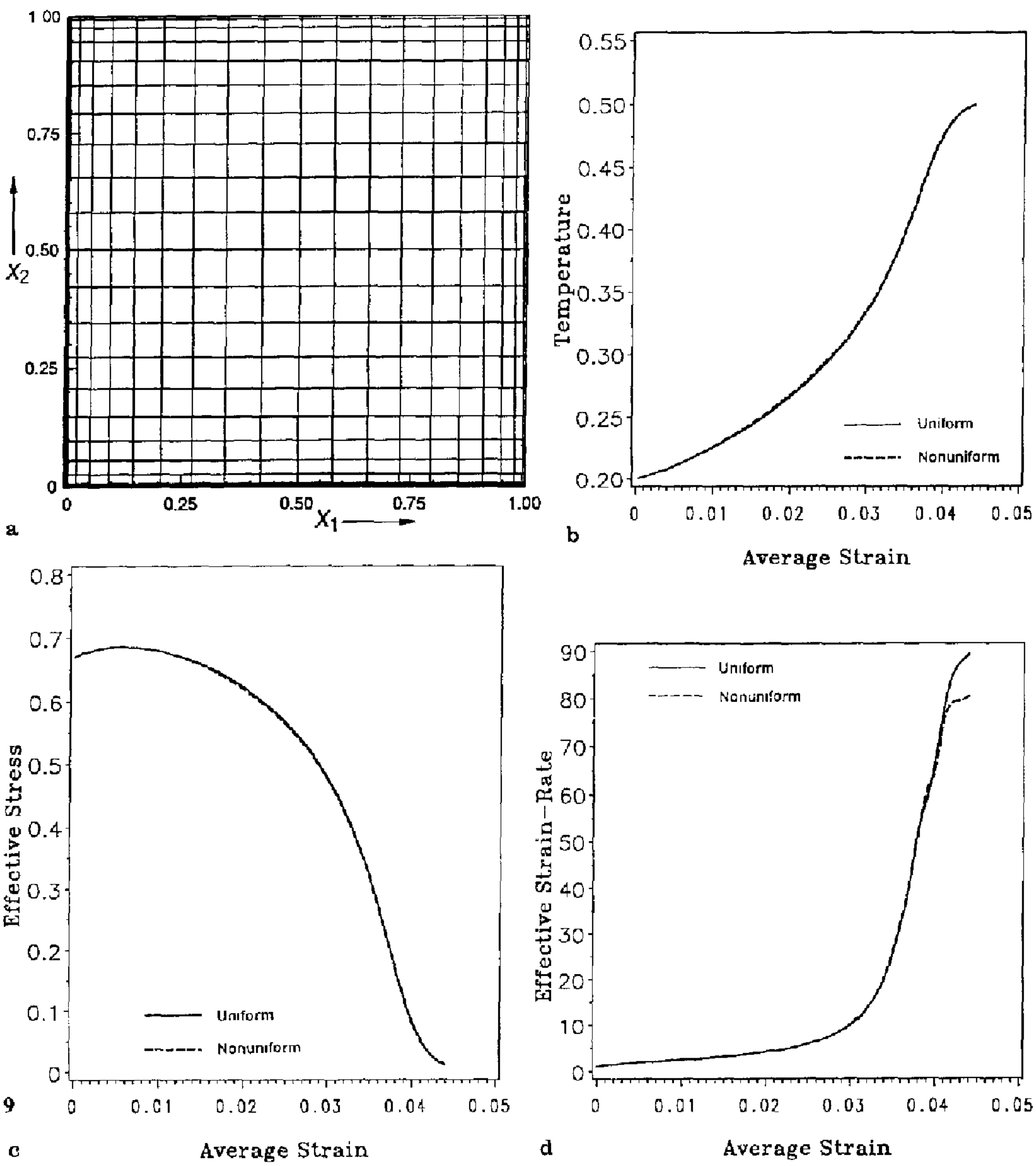

9

the element. We use Eq. (17) to evaluate g at the vertices of the quadrilateral element. The value g_n^* of the smoothened solution at the nth node is given by

$$g_n^* = \frac{1}{N_e} \sum_{m=1}^{N_e} g_{nm}, \tag{18}$$

where N_e equals the number of elements meeting at the node n, and g_{nm} equals the value of g at the nth node belonging to element m. Knowing g^* at each node, we can interpolate its value at any other point by using the finite element basis functions. The percentage error E in the deviatoric strain-rate tensor $\mathbf{D}$ defined by

$$E = \left(\frac{\|\mathbf{e}\|_0^2}{\|\mathbf{e}\|_0^2 + \|\mathbf{D}\|_0^2} \right) \times 100, \tag{19}$$

$$\mathbf{e} = \mathbf{D} - \mathbf{D}^*, \quad \|\mathbf{e}\|_0^2 = \sum_{m=1}^{N_{el}} \int_{\Omega_m} \mathbf{e}^{\mathrm{T}} \mathbf{e} \, d\Omega, \tag{20.1, 20.2}$$

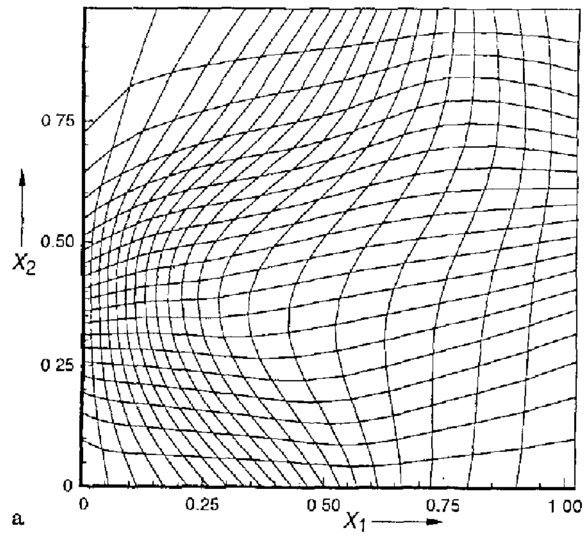

a

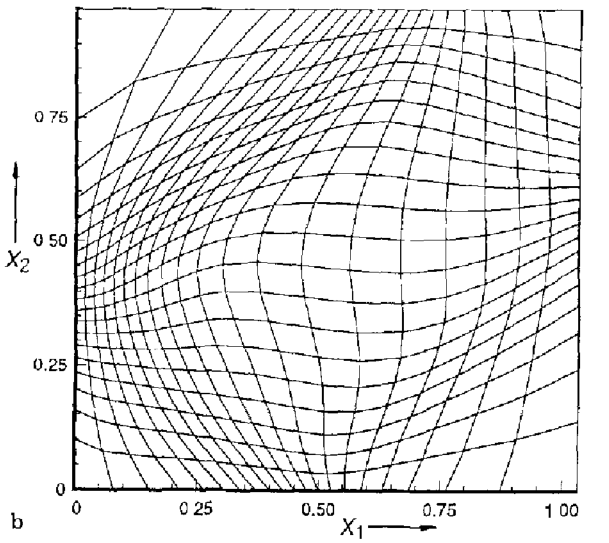

b

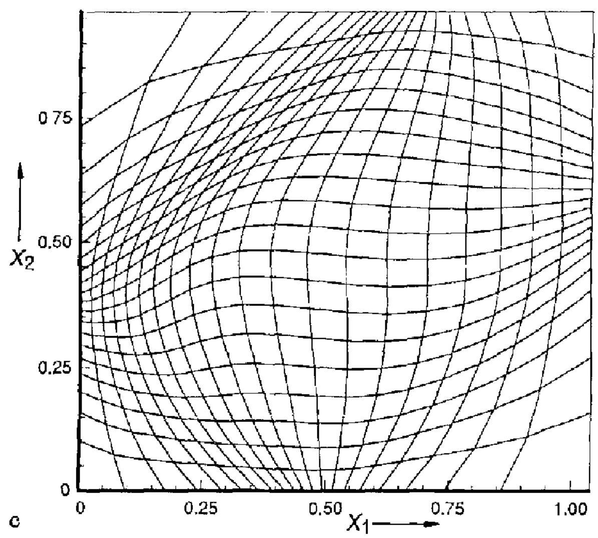

c

Fig. 10 a–c. Adaptively refined meshes at **a** $\gamma_{avg} = 0.02$, **b** $\gamma_{avg} = 0.03$, and **c** $\gamma_{avg} = 0.037$ when the deformation is expected to localize along the sides of a parallelogram where N_{el} equals the number of elements in the mesh, is plotted in Fig. 8. The error for the solution obtained by using the adaptively refined mesh is lower for $\gamma_{avg} \leqq 0.037$ and it then suddenly increases to match with that obtained for the solution computed by using a fixed mesh. It probably is due to the large errors caused by smoothening out of the approximate solution in the late stages of the band development when the deformations within the band are very intense. Batra and Ko (1992) found that, contrary to the intuitive thinking, the error as given by Eq. (19) was higher for the approximate solution computed by using a fixed mesh of three-noded triangular elements with 841 nodes as compared to that for a similar mesh with 441 nodes. They remarked that the error measure (19) is rather crude.

Since the adaptively refined meshes are obtained by repositioning the nodes, one might suspect that the solution so obtained will depend upon the initial mesh at time $t = 0$. That such is not case is confirmed by results depicted in Fig. 9 and obtained by using two different initial meshes, namely, a uniform mesh of 400 elements and a nonuniform mesh of 400 elements shown in Fig. 9a. The curves delineating the evolution at the origin of the temperature rise, effective strain-rate and the effective stress, and of the error measure (19) for the two solutions essentially coincide with each other. We note that the error measure is not plotted in Fig. 9.

In an attempt to study the interaction between bands originating from two different locations, Batra and Liu (1990) introduced two identical temperature perturbations with their centers

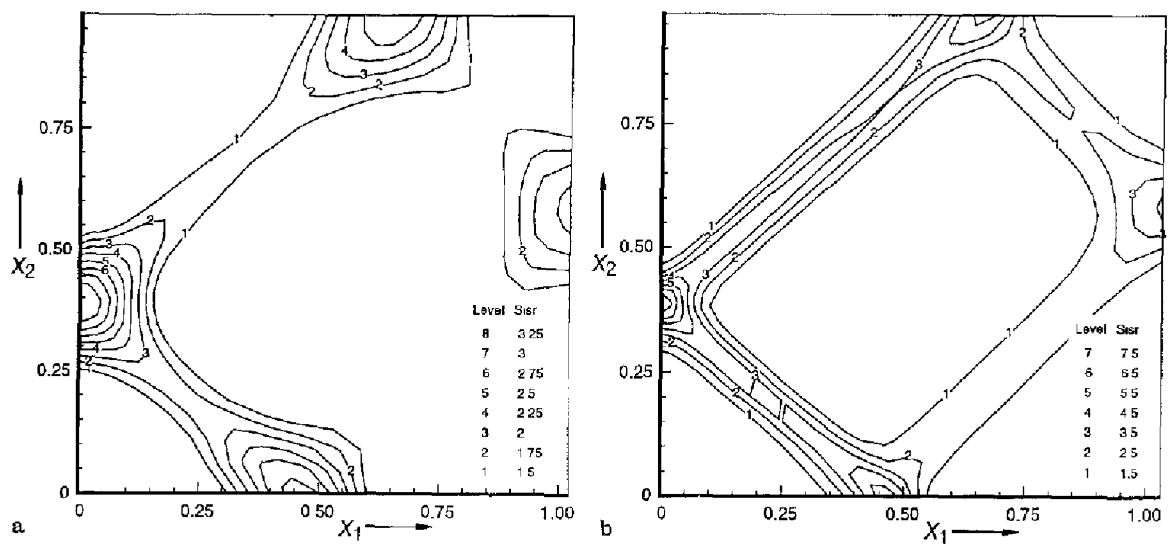

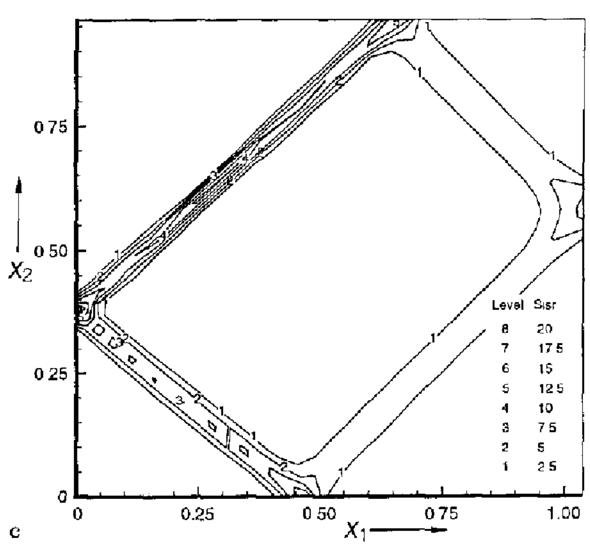

Fig. 11 a–c. Contours of the second invariant of the deviatoric strain-rate tensor at **a** $\gamma_{avg} = 0.02$, **b** $\gamma_{avg} = 0.03$, and **c** $\gamma_{avg} = 0.037$ when the center of the initial temperature bump is located at (0, 0.375) situated on the vertical centroidal axis and equidistant on either side of the horizontal centroidal axis. Assuming that the deformation of the block was symmetrical about the two centroidal axes, they studied deformations of the region in the first quadrant only and found that deformation localized into regions with their centerlines forming a parallelogram. We analyzed the problem defined in Sect. 2 except that the center of the temperature bump (10.2) is now located at (0, 0.375) rather than at the origin. The initial mesh consisted of 400 uniform quadrilateral elements, the meshes generated at $\gamma_{avg} = 0.02$, 0.03, and 0.037 by using the mesh refinement technique of Sect. 3 and depicted in Fig. 10 show that fine elements are generated within severely deformed regions and coarse elements elsewhere. The contours of the effective strain-rate plotted in Fig. 11 at $\gamma_{avg} = 0.02$, 0.03, and 0.037 show that the material along the side passing through the center of the temperature bump and making an angle of nearly 45° clockwise with the vertical line is deforming more severely than that along the other three sides of the parallelogram. Similar results were obtained by Batra and Liu (1990) who used a fixed mesh of nine-noded quadrilateral elements.

5 Conclusions

We have developed an adaptive mesh refinement technique that generates quadrilateral elements such that the integral of a deformation measure over an element is nearly the same for all elements in the mesh and all interior angles of the elements generated have values between 20° and 160°. The technique is easy to implement in an existing code since it only repositions the nodes and does not change the element connectivity. Values of solution variables at the relocated nodes are obtained by first determining to which element in the previous mesh a particular node belonged, and then interpolating values by using the finite element basis functions. The technique can be easily modified to generate triangular elements obtained by subdividing a quadrilateral into four triangles. Adaptively refined meshes when used to study the localization of the deformation into narrow bands in a thermally softening viscoplastic material give considerably sharper results as compared to those obtained by using a fixed mesh. Computed results for the shear band problem obtained by using adaptively refined meshes are found to be independent of the initial mesh used. The method was quite successful in analyzing the localization problem in which the deformation was expected to concentrate into narrow regions around the sides of a parallelogram.

Acknowledgements

This work was supported by the U.S. Army Research Office Grant DAAL03-91-G-0084 and the U.S. NSF Grant MSS9121279 to the University of Missouri-Rolla. Some of the computations were performed on the Ohio Supercomputer Center and the NSF Sponsored Supercomputer Center in Ithaca, NY.

References

Bai, Y.; Dodd, B. (1992): Adiabatic shear localization. Occurrence, theories and applications. New York: Pergamon Press

Batra, R. C.; Liu, D. S. (1989): Adiabatic shear banding in plane strain problems. J. Appl. Mech. 56, 527–534

Batra, R. C.; Kim, C. H. (1990): An adaptive mesh refinement technique for the analysis of adiabatic shear banding. Mech. Res. Commun. 17, 81–91

Batra, R. C.; Liu, D. S. (1990): Adiabatic shear banding in dynamic plane strain compression of a viscoplastic material. Int. J. Plasticity 6, 231–246

Batra, R. C.; Zhu, Z. G. (1991): Dynamic shear band development in a bimetallic body containing a void. Int. J. Solids Struct. 27, 1829–1854

Batra, R. C.; Ko, K. I. (1992): An adaptive mesh refinement technique for the analysis of shear bands in plane strain compression of a thermoviscoplastic solid. Computational Mech. 10, 369–379

Drew, D. A.; Flaherty, J. E. (1984): In: Gurtin, M. E. (ed): Phase transformations and material instabilities in solids, pp. 37–60. Academic Press

Hinton, E.; Campbell, J. S. (1974): Local and global smoothing of discontinuous finite element functions using a least squares method. Int. J. Num. Meth. Eng. 8, 461–480

Hughes, T. J. R. (1987): The finite element method. Linear static and dynamic finite element analysis. New York: Pergamon Press
Needleman, A. (1989): Dynamic shear band development in plane strain. J. Appl. Mech. 56, 1–9
Pervaiz, M. M.; Baron, J. R. (1988): Commun. Appl. Num. Meth. 4, 97–111
Safjan, A.; Demkowicz, L.; Oden, J. T. (1991): Adaptive finite element methods for hyperbolic systems with application to transient acoustics. Int. J. Num. Meth. Eng. 32, 677–707
Zhu, J. Z.; Zienkiewicz, O. C.; Hinton, O.; Wu, J. (1991): A new approach to the development of automatic quadrilateral mesh generation. Int. J. Num. Meth. Eng. 32, 849–886
Zienkiewicz, O. C.; Zhu, J. Z. (1991): Adaptivity and mesh generation. Int. J. Num. Meth. Eng. 32, 783–810

Communicated by S. N. Atluri, January 22, 1993